

# In vivo near-infrared spectroscopy of rat skin tissue with varying blood glucose levels

Jonathon T. Olesberg, Lingzhi Liu, Varlerie Van Zee, and Mark A. Arnold

Optical Science and Technology Center  
and Department of Chemistry  
University of Iowa, Iowa City, IA 52242, USA

## ABSTRACT

We have performed *in vivo* measurements of near-infrared rat skin absorption in the 4000–5000  $\text{cm}^{-1}$  spectral range (2.0–2.5  $\mu\text{m}$  wavelength) during a glucose clamp experiment. The goal of this work is to identify the presence of glucose-specific spectral information in order to evaluate the requirements for a noninvasive transcutaneous glucose instrument. Skin spectra are collected using an FTIR spectrometer coupled with a fiber-optic interface. In the experiment, an animal is allowed to stabilize at a euglycemic level for three hours while blood glucose values are monitored using samples taken from an arterial catheter. The blood glucose level is then increased above 30 mM by venous infusion of glucose and held for two hours, after which it is allowed to return to normal. Spectra are recorded continuously during the procedure and are analyzed to identify changes due to the glucose variations. Because the change in absorbance due to an increase in glucose concentration is small compared to changes due to other variations (e.g., the thickness of the skin sample), a simple subtraction of absorbance spectra from the hyperglycemic and euglycemic phases is not instructive. Instead, a set of principal components is determined from the euglycemic period where the glucose concentration is constant. We then examine the change in absorbance during the hyperglycemic period that is orthogonal to these principal components. We find that there are significant similarities between these orthogonal variations and the net analyte signal of glucose, which suggests that glucose spectral information is present.

**Keywords:** non-invasive, near-infrared, glucose, hyperglycemia, FTIR, spectroscopy, *in vivo*, skin

## 1. INTRODUCTION

Diabetes is one of the fastest growing diseases around the world. The World Health Organization estimates that 177 million people worldwide currently have diabetes and this number is projected to increase to more than 370 million people by the year 2030.<sup>1</sup> The costs associated with diabetes— which include premature death, pain, and financial burden— are tremendous. These costs are directly related to the medical complications associated with chronic hyperglycemia. Early detection and tight glycemic control are paramount to controlling the costs of the diabetes epidemic.<sup>2,3</sup>

The cornerstone to tight glycemic control is frequent glucose monitoring, where blood glucose concentrations are measured to help administer proper levels of insulin and maintain euglycemic conditions. Glucose sensing technology has advanced considerably in recent years, thereby providing excellent tools for home glucose monitoring and establishing opportunities for tight glycemic control. Unfortunately, the cost and pain associated with current glucose test-strip technology generally restrict the number of daily measurements performed by the average person with diabetes. Recent instrumental advances are focused on reducing these technological barriers. Examples of next-generation technologies include implantable glucose biosensors,<sup>4,5</sup> which are capable of continuous glucose monitoring over multiple days, and the GlucoWatch biographer, which provides a new glucose reading every 20 minutes.<sup>6</sup>

Noninvasive optical sensing of glucose has been proposed by many research groups for the frequent and painless measurement of glucose in people with diabetes.<sup>7</sup> The concept is to pass a selected band of near-infrared

---

Further author information:

J.T.O: E-mail: jonathon-olesberg@uiowa.edu, Telephone: 319-335-3514

M.A.A.: E-mail: mark-arnold@uiowa.edu, Telephone: 319-335-1368

radiation through a vascular region of the body and extract the glucose concentration from the resulting spectral information. Near-infrared spectroscopy is the principal approach for this noninvasive glucose sensing because of the unique near-infrared absorption spectrum of glucose and the significant penetration of near-infrared light into human tissue.

To date, all reported attempts to measure glucose noninvasively with near-infrared spectroscopy have involved collecting spectra from human subjects and using multivariate calibration techniques to correlate variations in the spectral information to blood glucose concentrations.<sup>8-17</sup> Partial least squares regression (PLS) is the most popular multivariate calibration algorithm for this purpose. PLS relies on a regression step in which spectral variance is statistically correlated with assigned glucose concentrations. For the most part, published accounts fail to convincingly prove that concentration predictions from these multivariate calibration models are based on glucose-specific spectral information, as opposed to chance correlations within the data set.<sup>7,18</sup> This is a problem because the PLS algorithm is designed to accentuate *all* signals that even weakly correlate with analyte concentration. Basically, the PLS algorithm cannot distinguish or enhance glucose-specific spectral variations relative to all other sources of spectral variation that happen to correlate with concentration. Unfortunately, it is common to generate apparently functional PLS calibration models on the basis of non-analyte dependent variance, such as noise and spectrometer drift. This problem is particularly troublesome when the glucose concentration varies systematically as a function of time.

The primary goal of this work is to identify glucose-specific absorbance features in *in vivo* spectra in order to establish a solid analytical grounding for evaluating glucose calibration models generated with multivariate techniques. An auxiliary goal is to gather evidence toward answering the question of the distribution volume of glucose in tissue. At question is whether intracellular glucose concentrations track with extracellular and capillary glucose concentrations, especially during large concentration variations. The answer has significant implications for a transcutaneous measurement where the ratio of intracellular to extracellular volume is 2:1.

## 2. EXPERIMENT

Adult male Sprague Dawley rats were used as an animal model in this work. Previous studies in our laboratory have demonstrated that the skin on the upper shoulders of these animals has similar absorption properties to that of a skin fold on the back of a human hand. Retired breeders rats weighing more than 400 g were used. The animals were anesthetized using sodium pentobarbital for the surgical preparation. Anesthesia was maintained during the course of the procedure by administration of chloralose. A catheter was placed in the right femoral vein for the infusion of glucose, saline, and anesthetic during the experiment. The right femoral artery was cannulated to provide access to the arterial blood stream.

Rats were fasted overnight prior to the clamp experiments. After anesthetization, rectal temperature and pulse-oximetry probes were inserted to monitor animal temperature, pulse rate, and oxygenation during the cannulation procedure, which was performed on a heated surgical station. After surgery, the animal was transferred to the spectroscopy station. Animal temperature was maintained at 38.0 °C using a closed-loop temperature controller. Pulse rate and oxygenation were monitored continuously. Supplemental oxygen was provided to the animal at a rate of approximately 1 L/min.

Tissue spectra were collected using a Nicolet Nexus FTIR spectrometer. Spectra were collected continuously through a skin fold on the animal's back. A 50 W tungsten-halogen bulb with an integrated, gold-coated reflector was used as a broad-band light source. A custom fiber optic interface was used to bring light from the spectrometer to the animal and to couple the transmitted light to an external detector. A 1 mm diameter solid-core low-OH silica fiber terminated with a 4 mm sapphire ball lens was used for light delivery to the skin fold. Transmitted light was collected using a second ball lens into another solid-core fiber. The light was then coupled using an aspheric lens pair onto a two-stage thermoelectrically-cooled extended-wavelength InGaAs detector with a 2.6  $\mu\text{m}$  cutoff. The detector was coupled to a low-noise variable-gain transimpedance amplifier, the output of which was connected to the external detector port of the spectrometer. Spectra were recorded as 60 s averages with 16  $\text{cm}^{-1}$  (8 nm) spectral resolution.

After the fiber-optic interface was attached to the animal, spectra were collected for approximately 3 hours while the blood glucose levels were held constant. During this time, isotonic saline was infused into the venous

line at 2 mL/hr. After a sufficient set of baseline spectra were collected, a 50% glucose solution was infused at a rate of 2 mL/hr for 2 hours. After that, glucose infusion was stopped and saline infusion was resumed.

Blood samples were collected from the arterial cannula at 5–15 minute intervals. Arterial glucose readings were measured using a HemoCue<sup>®</sup> Glucose 201 Analyzer. When blood glucose values exceeded the functional range of the device (24 mM), the blood samples were diluted with saline. Calibrations were performed with a set of diluted and non-diluted blood samples within the functional range of the device to correct for a proportional error due to the reduction of hematocrit in the diluted samples.

### 3. RESULTS

#### 3.1. Aqueous Path Length Estimation

Skin tissue can vary significantly in thickness from animal to animal and for different sampling sites on a single animal. In addition, the thickness of a skin fold can be modified by varying the pressure applied to the tissue. In order to account for these variations, we use an estimation of the aqueous path length based on a simple linear regression of the tissue absorbance spectra in terms of the known absorptivities of water, type-I collagen, keratin, and fat. In order to account for variations in the total skin scattering losses and temperature variation, a constant spectrum and a linearly varying spectrum are also included. An example absorbance spectrum with the regressed fit is shown in Figure 1. The primary structure of the measured spectra is reproduced by the fit, although there is some deviation around the fat absorption features at 4250 and 4350  $\text{cm}^{-1}$ . Aqueous path lengths can be extracted reliably using this approach because water is the dominant absorptive component in tissue (water is responsible for the overall parabolic-like shape of the spectrum). The effective aqueous path length for all of the spectra in this study were  $0.70 \pm 0.04$  mm.

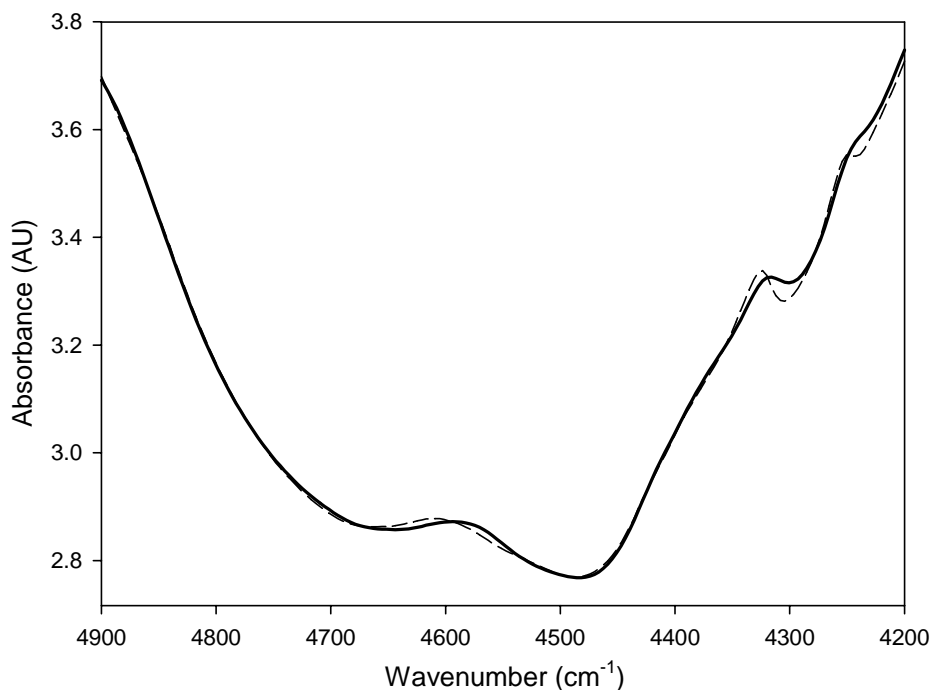


**Figure 1.** Measured (solid) and regressed spectra (dash). The purpose of the regression is solely to estimate the effective aqueous path length of the tissue.

### 3.2. Net Analyte Signal Analysis

The primary goal of the work is to identify glucose spectral features in the *in vivo* tissue spectra. In principle, one would think that it should be possible to reference spectra from a time period with high glucose concentration to a spectrum with low glucose concentration. However, this does not work in practice because of the very small absorption amplitude of glucose (on the order of 14  $\mu$ AU for a 1 mM change in glucose concentration) and the large variations in tissue absorbance due to other factors (e.g., water and protein content). In our experience, it is extremely difficult to avoid changes in tissue absorbance properties even when trying to maintain a constant fiber-optic sampling position, pressure, and sample thickness. Compounding these difficulties is the fact that it takes 10's of minutes to induce a significant change in the animal's arterial glucose level, in addition to the time required for glucose transport from the core blood stream into the peripheral skin volume.

Instead of trying to eliminate spectral variations experimentally, it is possible to quantify those variations and look for changes that appear in the high-glucose spectra that are not described by the variations observed in the constant-glucose baseline spectra. This procedure is a generalization of the simple subtraction described above. Instead of subtracting a single spectrum, however, a subspace of spectra is used.

An optimal subspace that incorporates the primary systematic variations in a set of spectra can be obtained from a principal component analysis. Mathematically, this can be performed using a singular-value decomposition of a matrix that is comprised of the spectra concatenated as columns. If the matrix of spectra is denoted as  $A$ , a singular-value decomposition can be written as

$$A = UWV^T \quad (1)$$

where  $U$  is a matrix of orthonormal vectors that are the principal components of  $A$ ,  $W$  is a diagonal matrix of singular-values, and  $V$  is a square orthogonal matrix. The columns of  $U$  are commonly referred to as principal components, basis-vectors, or factors. The column corresponding to the largest singular value describes the largest systematic variation in the spectra in  $A$ . Subsequent columns (ordered by decreasing singular values) describe less significant variations (in a least-squares sense), until, after a certain number of factors, the remaining variations are dominated by noise. The number of significant factors depends on the sample under investigation and the noise characteristics of the spectroscopy system. Experimentally, the spectral variations described by the principal components are due to variations in tissue composition induced by the pressure of the clamp (e.g., water and protein content), variations in animal physiology, and instrumental drift.

After identifying a set of factors that describe the systematic (non-noise) variations in the baseline spectra, additional variations not described by the principal components can be identified by removing the projection of the a spectrum onto the baseline factors from that spectrum. If a matrix  $H$  consists of a column-wise concatenation of spectra from the high-glucose portion of the experiment, the portion of  $H$  that is orthogonal to the subspace defined by the columns of  $U$  can be written as

$$H_{\perp} = (I - UU^+)H \quad (2)$$

where  $I$  is the identity matrix and  $U^+$  is the Moore-Penrose pseudoinverse of  $U$ . In this study,  $H_{\perp}$  is any change in the tissue absorbance observed for high-glucose concentrations that has not already been observed in the baseline spectra.

Figure 2 shows the time profile of arterial glucose concentration in the animal over the course of the experiment. The lower gray regions on the figure indicate the times over which spectra were used to form the baseline (11:00–14:05 and 17:30–18:00). The latter set of spectra are included in the calculation of the baseline factors in order to correct for long-term drift. Spectra collected between 15:20–16:00 are used as the representative high-glucose spectra. In the period between 13:00–13:45, the fiber-optic clamp was repositioned on the animal between each scan. This was done in order to observe variations due to interface placement and pressure into the baseline spectra and to reduce the impact of unintentional variations during the high-glucose portion of the experiment.

A principal component analysis was performed on the baseline spectra. It was determined that a set of eight factors described the majority of the non-glucose systematic variations in the spectra. The number of factors was

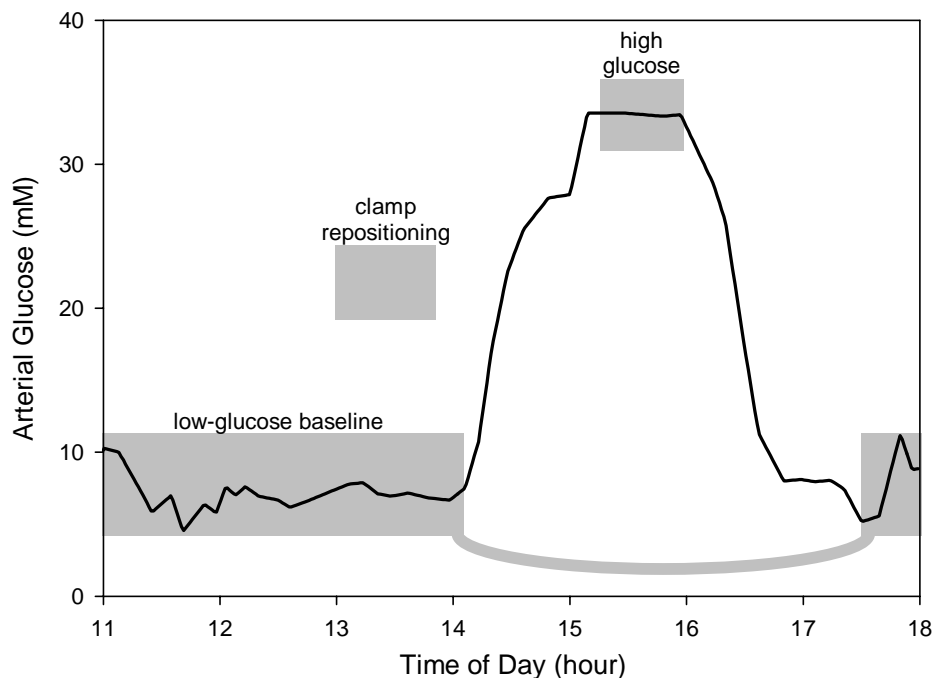


**Figure 2.** The solid line shows the arterial glucose concentrations over the course of the experiment. The gray rectangles indicate the division of experiment into low-glucose baseline and high-glucose time periods. In the time between 13:00–13:45, the fiber optic interface was repositioned on the animal between each scan.

chosen based on a visual inspection of the residuals after removing the eight factors. The choice was confirmed by plotting the root-mean-square (RMS) of the residual absorbance over the  $4200\text{--}4900\text{ cm}^{-1}$  wavenumber range, as shown in Figure 3. There is a break in the slope occurring at factor eight, which suggests that is the transition from factors describing systematic variations to factors describing noise.

These eight factors define a subspace that contains the vast majority of spectral variance observed in the experiment. When these factors are removed from the spectra for which the animal’s glucose concentration was high, significant residual structure remains. The average residual after the subtraction of the baseline factors is shown as the solid line in Figure 4. The residual has structure that does not appear to be due to noise. The dashed line in Figure 4 is the absorbance spectrum of glucose. There is some similarity between them, with peaks around  $4700$ ,  $4400$ , and  $4300\text{ cm}^{-1}$ , but it is not obvious that the spectral residual is due to glucose.

A much stronger similarity is seen if the residual high-glucose spectrum is compared to the pure component spectrum of glucose after the same baseline factors have been removed from the glucose absorbance spectrum. The result is shown as the dash-dot line in Figure 4. The difference between the original glucose absorbance spectrum and the reduced glucose absorbance (after the factors have been removed) is due to the requirement that the remainder be orthogonal to the baseline factors.

The residual spectrum after the removal of the baseline factors from the glucose absorbance spectrum is simply the net analyte signal, as defined by Lorber.<sup>19,20</sup> The net analyte signal is the portion of the analyte absorption that is orthogonal to all other variations in the sample matrix (including absorbance due to other chemical components, effects such as those due to temperature variations, and instrumental variations). The similarity of the residuals of the high-glucose spectra to the net analyte signal of glucose is evidence of glucose-specific spectral information in the *in vivo* spectra.

The net analyte signal can be used to directly quantify the analyte concentration. In the case of an ideal multivariate calibration, the calibration spectrum from a method such as PLS should be identical to the net

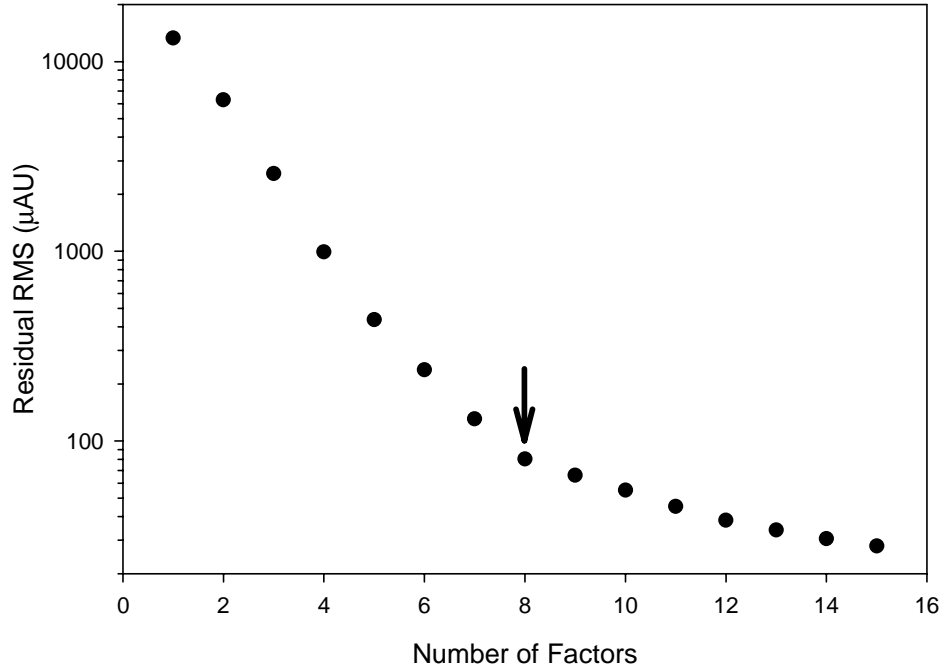


**Figure 3.** RMS of the spectral residuals after removal of indicated number of factors. Based on the break in the slope, an eight-factor basis is used in the analysis.

analyte signal, though in practice, they will differ. Both the net analyte signal and the PLS calibration spectrum are *estimations* of the ideal calibration spectrum. The PLS calibration spectrum is calculated using a statistical regression of the analyte concentrations with the PLS factors, while the net analyte signal is calculated using the analyte absorbance spectrum and a set of baseline factors. In general, the PLS calibration will be more optimized because of the regression step, but the net analyte signal approach provides a more robust calibration because it is based directly on analyte absorption information.

A properly-scaled calibration spectrum can be generated from the net analyte signal using the known absorptivity of the analyte:

$$\beta = \frac{n}{n \cdot g}, \quad (3)$$

where  $\beta$  is the scaled calibration spectrum,  $n$  is the net analyte signal, and  $g$  is the absorptivity spectrum of glucose. The predicted glucose concentration can then be calculated as

$$c = \frac{a \cdot \beta}{\ell} + \overline{c_{BL}}, \quad (4)$$

where  $a$  is the absorbance spectrum of the sample being quantified,  $\ell$  is the aqueous path length, and  $\overline{c_{BL}}$  is the average concentration of the baseline spectra.

The results of this procedure are shown in Figure 5, where the open circles are for the spectra used in the calculation of the baseline factors and the solid circles are predictions for spectra not in the baseline set. The significant scatter in the period between 13:00–13:45 is due to added spectral variability caused by moving the fiber-optic interface between scans. The predicted glucose concentrations follow the arterial glucose trend with a 20-minute delay. The RMS prediction error for the baseline spectra is 3.1 mM, including the time period between 13:00–14:45. The prediction error for the non-baseline region is 6.4 mM. A significant portion of the non-baseline prediction error is due to the time-lag between the arterial and optically predicted values. If the predicted values are compared to arterial values from 20 minutes earlier, the RMS error drops to 2.6 mM. The

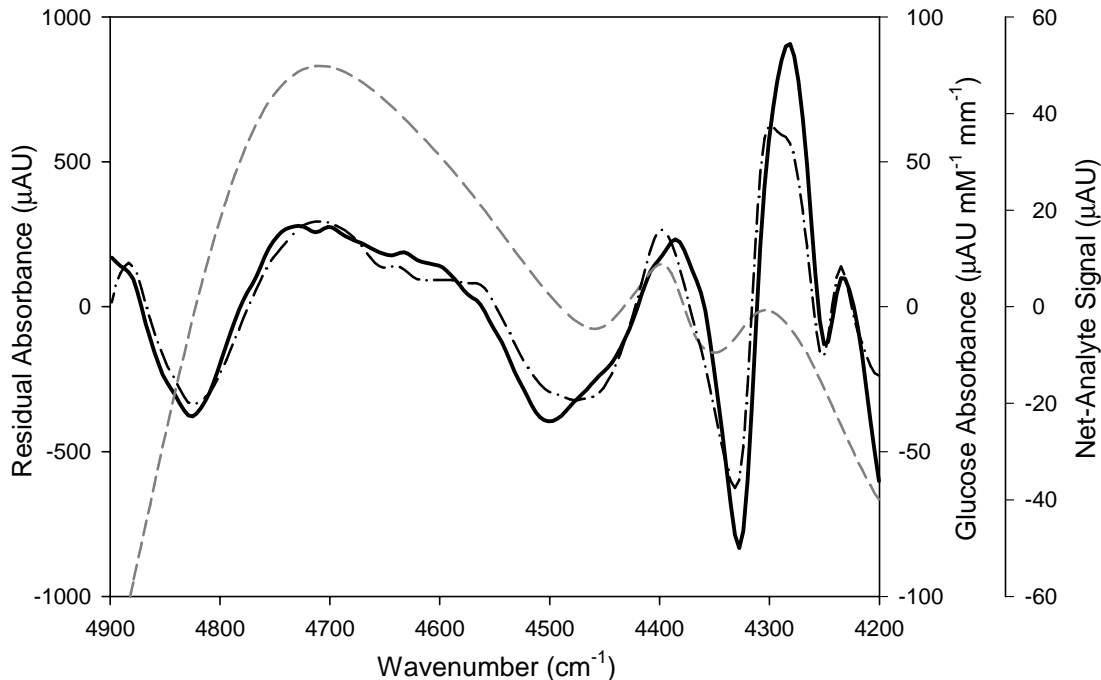


**Figure 4.** Spectral residuals after the removal of eight baseline factors from spectra collected while the glucose concentration was elevated (solid). Absorbance spectrum of pure glucose (dash). Glucose absorbance after the removal of the eight baseline factors (dash-dot).

magnitude of the prediction errors is obviously too large for clinical use at this point. However, our emphasis to date has been on obtaining analytical glucose-specific information. We believe that accuracy can be improved as the design of our experiment and equipment improves.

It should be emphasized that the scaling of the predicted glucose values is derived entirely from the amplitude of the absorptivity spectrum of glucose and not from a regression. This suggests that the glucose concentration exists throughout the aqueous volume of the tissue (extracellular and intracellular regions). We believe this to be a significant result as the precise dynamics of glucose uptake into the cells and glucose metabolism once inside the cell are not fully known.

### 3.3. Partial Least-Squares Analysis

A more traditional PLS analysis of the *in vivo* spectra has also been completed using normal precautions against overmodeling. A set of 54 randomly selected spectra were removed from the data set and set aside for an independent measure of the standard error of prediction. The remainder of the spectra (306) were used to build the calibration. The number of factors was chosen by performing 50 shuffles of a leave-one-third-out cross-validation. Eight factors were determined to be optimal, which is consistent with the previous net analyte signal calibration. The resulting PLS calibration spectrum is shown in Figure 6 along with the net analyte signal spectrum. The major features are reproduced in both spectra, although there are slight differences in feature width and location. Note also that there is little high-frequency noise-like structure in the PLS calibration spectrum. Such noise-like structure is often an indication of overmodeling.

Glucose concentrations determined from the calibration and prediction spectra are shown in Figure 7. Predictions using spectra from the calibration set are shown as open circles, while those from the prediction set are shown as solid circles. A similar time delay is seen as in the net analyte signal calibration. The standard error of calibration is 4.2 mM and the standard error of prediction is 3.9 mM.

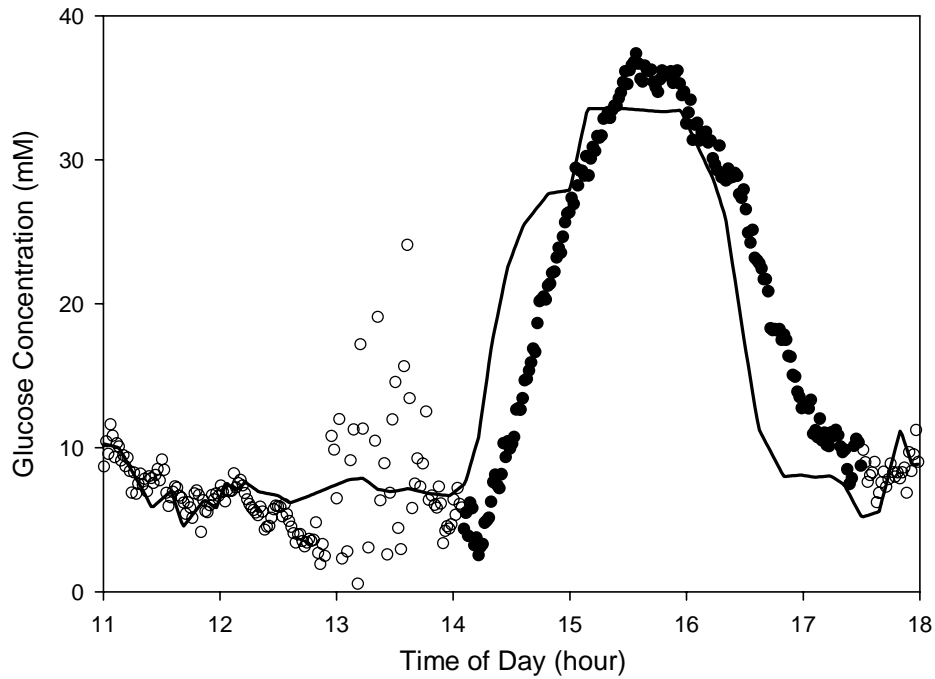


**Figure 5.** Predicted glucose concentrations using the net analyte signal. The open circles are predictions for the baseline spectra. The solid circles are for the non-baseline spectra. The solid line is the arterial blood glucose concentration measured with a glucose analyzer.

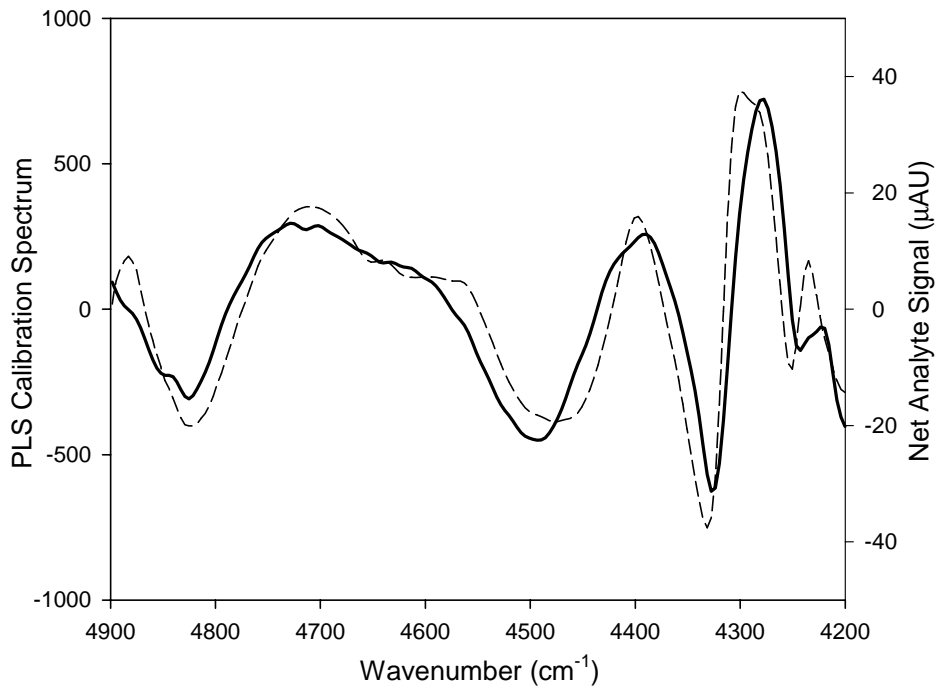


**Figure 6.** Calibration spectrum generated by the PLS calibration (solid). Net analyte signal for glucose (dash).

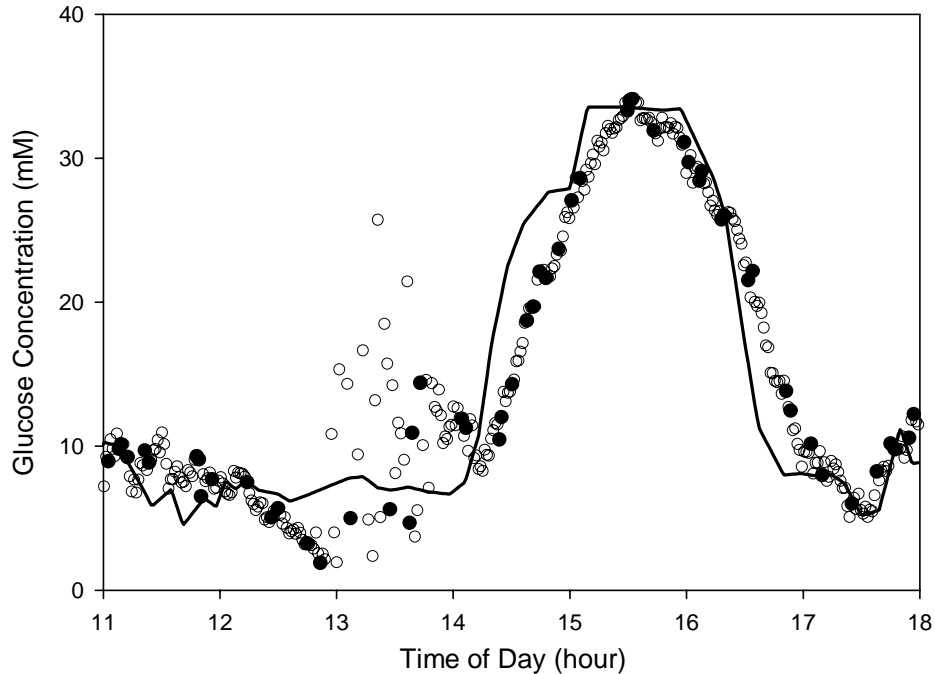


**Figure 7.** Predicted glucose concentrations using PLS. The open circles represent predictions based on spectra from the calibration set. The solid circles are for the independent prediction spectra, which were not used in the model-building process.

#### 4. CONCLUSIONS

We have performed *in vivo* measurements of rat skin absorbance during a glucose clamp experiment. By removing the projection of spectra with high glucose concentration onto a set of eight baseline factors, we observe significant spectral differences between high- and low-glucose spectra.

By comparing these differences to the net analyte signal of glucose with respect to the sample set of factors, we have identified glucose-specific features in these *in vivo* spectra. This structure provides a picture of what a valid PLS calibration spectrum should look like for this experiment.

A calibration spectrum was determined by scaling the net analyte signal. This calibration was based solely on the set of baseline spectra with near-constant glucose concentration and the absorbance of glucose. When applied to the measured spectra, the RMS error for the non-baseline spectra was 6.4 mM. If allowance is made for a 20-minute delay between the blood and tissue concentrations, the RMS error is 2.6 mM. The scaling of this calibration was based entirely on the absorptivity of glucose with no slope correction or regression of the predicted vs. known concentrations. The amplitude of the predicted values is consistent with glucose being distributed throughout the entire aqueous volume (intracellular *and* extracellular fluids).

Calibration spectra determined using PLS are very consistent with the net analyte signal of glucose, which suggests that the PLS model generated for this experiment is based on glucose-specific information and not on secondary effects, such as changes in scattering or chance correlations.

The current experiment procedure was designed to minimize the variance in the *in vivo* spectra. The experiments are very short-term in nature (approximately 7 hours), involve only a single animal, require a large set of baseline spectra, and involve primarily one tissue site. Ongoing work is addressed at relaxing these constraints in a systematic manner and examining how each factor affects the net analyte signal.

## ACKNOWLEDGMENTS

The authors wish to acknowledge Judy Herlein of the VA Medical Center of Iowa City and Donald Morgan of the University of Iowa Department of Medicine for their gracious assistance with the design and implementation of the rat glucose clamp procedure. This research was supported by grants from the National Institute of Diabetes and Digestive and Kidney Diseases of the National Institutes of Health (DK-60657 and DK-02925).

## REFERENCES

1. <http://www.who.int/ncd/dia/databases4.htm>.
2. D. Control and C. T. R. Group, "The effect of intensive treatment of diabetes on the development and progression of long-term complications in insulin-dependent diabetes mellitus," *N. Engl. J. Med.* **329**, pp. 977–986, September 1993.
3. *Diabetes in America*, NIH Publication No. 95-1468, National Institutes of Health, National Institute of Diabetes and Digestive and Kidney Diseases, 2<sup>nd</sup> ed., 1995.
4. B. Feld, R. Brazg, S. Schwartz, and R. Weinstein, "A continuous glucose sensor based on wired enzyme technology— results from a 3-day trial in patients with type I diabetes," *Diabetes Technol. Ther.* **5**, pp. 769–777, 2003.
5. G. S. Wilson, "Making an imprint on blood glucose monitoring," *Nat. Biotechnol.* **15**, pp. 322–323, 1997.
6. J. A. Tamada, S. Garg, L. Jovanovic, K. R. Pitzer, S. Fermi, and R. O. Potts, "Noninvasive glucose monitoring: Comprehensive clinical results," *JAMA* **282**, pp. 1839–1844, 1999.
7. O. S. Khalil, "Spectroscopic and clinical aspects of noninvasive glucose measurements," *Clin. Chem.* **45**, pp. 165–177, 1999.
8. M. R. Robinson, R. P. Eaton, D. M. Haaland, G. W. Koeppe, E. V. Thomas, B. R. Stallard, and P. L. Robinson, "Noninvasive glucose monitoring in diabetic patients: A preliminary evaluation," *Clin. Chem.* **38**, pp. 1618–1621, 1992.
9. R. Marbach, T. H. Koschinsky, F. A. Gries, and H. M. Heise, "Noninvasive blood glucose assay by near-infrared diffuse reflectance spectroscopy of the human inner lip," *Appl. Spectrosc.* **7**, pp. 875–881, 1993.
10. H. M. Heise, R. Marbach, T. H. Koschinsky, and F. A. Gries, "Noninvasive blood glucose sensors based on near infrared spectroscopy," *Artif. Organs* **18**, pp. 439–447, 1994.
11. H. M. Heise, "Noninvasive monitoring of metabolites using near infrared spectroscopy: State of the art," *Horm. Metab. Res.* **28**, pp. 527–534, 1996.
12. K. U. Jagemann, C. Fischbacher, K. Danzer, U. A. Müller, and B. Mertes, "Application of near-infrared spectroscopy for non-invasive determination of blood tissue glucose using neural networks," *Z. Physikalische Chemie* **191**, pp. 179–190, 1995.
13. C. H. Fischbacher, K. U. Jagemann, K. Danzer, U. A. Müller, L. Papenkordt, and J. Schöler, "Enhancing calibration models for non-invasive near-infrared spectroscopical blood glucose determination," *Fresenius J. Anal. Chem.* **359**, pp. 78–82, 1997.
14. J. J. Burmeister, M. A. Arnold, and G. W. Small, "Noninvasive blood glucose measurements by near-infrared transmission spectroscopy across human tongues," *Diabetes Technol. Ther.* **2**, pp. 5–16, 2000.
15. A. Samann, C. H. Fischbacher, K. U. Jagemann, K. Danzer, J. Schöler, L. Papenkordt, and U. A. Müller, "Non-invasive blood glucose monitoring by means of near infrared spectroscopy: investigation of long-term accuracy and stability," *Exp. Clin. Endocrin. Diabetes* **108**, pp. 406–413, 2000.
16. S. F. Malin, T. L. Ruchti, T. B. Blank, S. N. Thennadil, and S. L. Monfre, "Noninvasive prediction of glucose by near-infrared diffuse reflectance spectroscopy," *Clin. Chem.* **45**, pp. 1651–1658, 1999.
17. K. Maruo, M. Tsurugi, M. Tamura, and Y. Ozaki, "In vivo noninvasive measurement of blood glucose by near-infrared diffuse-reflectance spectroscopy," *Appl. Spectrosc.* **57**, pp. 1236–1244, 2003.
18. M. A. Arnold, J. J. Burmeister, and G. W. Small, "Phantom glucose calibration models from simulated noninvasive human near infrared spectra," *Anal. Chem.* **70**, pp. 1773–1781, 1998.
19. A. Lorber, "Error propagation and figures of merit for quantification by solving matrix equations," *Anal. Chem.* **58**, pp. 1167–1172, 1986.
20. A. Lorber, K. Faber, and B. R. Kowalski, "Net analyte signal calculation in multivariate calibration," *Anal. Chem.* **69**, pp. 1620–1626, 1997.